Neurology Asia 2026; 31(1) : 275 – 285

Fat-suppressed T2-weighted fluid attenuated inversion recovery MR images allow efficient skull stripping in brain tumors using a brain extraction tool

*[1]Xiaowei Chen *PhD*, *[2]Rifeng Jiang *PhD*, [3]Jun Liu *BSc*, [3]Yu Jiang *BSc*, [3]Fengting Zhu *MSc*, [3]Yuquan Zheng *BSc*, [2]Wanyi Zheng *PhD*, [3]Haoqiang He *MSc*, [3]Yanchun Lv *PhD*, [3]Chuanmiao Xie *PhD*, [3]Changliang Su *PhD*, [3]Dongdong Huang *BSc*
*XW Chen and RF Jiang contributed equally to this work and are co-first authors.

[1]Department of Radiology, The Central Hospital of Wuhan, Tongji Medical College, Huazhong University of Science and Technology, Hubei, China; [2]Department of Radiology, Fujian Medical University Union Hospital, Fuzhou, China; [3]Department of Medical imaging, State Key Laboratory of Oncology in South China, Guangdong Provincial Clinical Research Center for Cancer, Sun Yat-sen University Cancer Center, Guangzhou, China.

Abstract

Objective: To explore the efficacy of fat-saturated T2-weighted fluid attenuated inversion recovery MRI (fs-FLAIR) in skull stripping for the treatment of brain tumors. *Methods:* MR images of brain tumors (gliomas, N=46; meningioma, N=51) were retrospectively collected, in which MRI protocols included contrast-enhanced T1-weighted MRI (T1C), fs-FLAIR or non-fs FLAIR MRI (nfs-FLAIR), T1-weighted MRI (T1), and T2-weighted fast spin echo MRI (T2). Skull stripping was implemented using the Brain Extraction Tool (BET) and evaluated with the Dice similarity coefficient as a comparison to manually segmented brain areas. To test the differences in Dice coefficients across different MR modalities, paired t tests and independent t test were utilized. Spearman's correlation analysis was used to determine the correlations between Dice coefficients and scanning parameters. *Results:* No significant correlations were observed between Dice coefficients and scanning factors influencing image contrast in the fs-FLAIR images of the two datasets, whereas significant correlations were observed with T1, T1C, T2, and nfs-FLAIR images. In gliomas, fs-FLAIR has the best skull-stripping performance, and the Dice coefficients were generally greater than 0.80 (maximum of 0.90). In contrast, most Dice coefficients were less than 0.8 in other sequences. All Dice coefficients of the fs-FLAIR images were significantly greater than those of T1, T2, and T1C images ($p < 0.0001$). Similar skull-stripping performances were observed in fs-FLAIR images of meningiomas and gliomas. Moreover, compared with nfs-FLAIR, fs-FLAIR resulted in higher Dice coefficients, with a maximum Dice coefficient of 0.87.
Conclusion: Fs-FLAIR allows fast and accurate skull stripping for brain tumors, and has the potential to aid in the development of intelligent diagnosis methods for these tumors.

Keywords: Magnetic resonance imaging, fat saturation, T2 fluid-attenuated inversion recovery imaging, skull stripping, brain tumors.

INTRODUCTION

Brain tumors strongly threaten human life and impose a great burden on society.[1] The stubbornly high cancer incidence has resulted in heavy workloads for health care systems.[2] MRI provides excellent contrast in detecting soft tissue, thus providing vital information for computer-aided diagnosis.[3] Nonbrain tissue components, such as skin, fat, skull, and eyeballs, hinder intelligent diagnosis; therefore, they strongly affect the running speed and prediction performance of automatic analysis techniques.[4,5] Inaccurate skull stripping reduces the accuracy of subsequent image processing, model building, and prediction performance.[6] Accurate skull stripping is highly

Address correspondence to: Dongdong Huang, Changliang Su, Chuanmiao Xie, Department of Medical imaging, State Key Laboratory of Oncology in South China, Guangdong Provincial Clinical Research Center for Cancer, Sun Yat-sen University Cancer Center, Guangzhou, 510060 China. Email: DD Huang, huangdd0618@163.com; CL Su, suchangliang2008@163.com; CM Xie, xchuanm@sysucc.org.cn

Date of Submission: 10 August 2025; Date of Acceptance: 12 December 2025
https://doi.org/10.54029/2026yis

required as an essential preprocessing step in computational neuroimaging, and stripping nonbrain tissues facilitates computer-aided management.[7]

Technically, skull-stripping can be performed manually, semiautomatically, or automatically.[8] Manual segmentation, the gold standard for brain extraction, can be extremely time-consuming.[9] Skull stripping using automatic methods such as deformable surface-based methods, mathematical morphology-based methods, and atlas/template-based methods is more efficient and repeatable.[10] Brain surface extraction (BSE) is a skull stripping technique based on mathematical morphology. In images with poor contrast, the extraction effect of BSE is poor, which is a disadvantage because it is based on edge detection.[10] The robust learning-based brain extraction (ROBEX) system fits the optimal contour using discriminative models and generative models; this system exhibits favorable adaptability but is associated with relatively high costs.[11] SynthStrip primarily adopts deep learning strategies and achieves skull stripping for various brain images by synthesizing a large number of virtual training images, enabling adaptation to different imaging conditions and image qualities. However, it has relatively high hardware requirements.[4]

Although automatic skull-stripping from MRI can facilitate intelligent diagnosis, currently available skull stripping methods have been developed primarily for brains without pathological abnormalities.[12] Tumor-bearing brain MR images have more complicated morphological features, that could potentially reduce the accuracy of brain extraction.[13] Multiparametric MRI (mp-MRI), including contrast-enhanced T1-weighted MRI (T1C), T2 fluid attenuated inversion recovery MRI (FLAIR), T1-weighted MRI (T1) and T2-weighted fast spin-echo MRI (T2), are routinely used for the diagnosis of brain tumors in the clinic[14], and almost all of these brain extraction techniques utilize the abovementioned MRI sequences for single- or multimodality studies.[15,16] Compared with 3D T1-weighted MRI with an isotropic acquisition of 1 mm, traditional thick-layer MRI with a slice thickness of approximately 5 mm is considerably more time-saving. However, it is difficult to achieve satisfactory skull stripping using this method. Moreover, the prediction performance of brain extraction algorithms might interfere with the nonuniformity of MRI scanning parameters among multiple centers, thereby limiting their transferability.[17]

Although many researchers have proposed complex methods and algorithms to extract the brain from MR images[10], the applicability of these methods to thick-layer MR images has not been fully demonstrated to date.[18] Hence, exploring fast and robust skull-stripping methods to obtain thick-layer MR images of brain tumors is valuable. FLAIR is a popular and widely applied MRI sequence in clinics, as introduced by Hajnal *et al*.[19] With a long echo time (TE) and long inversion time, FLAIR can suppress signals from cerebrospinal fluid (CSF) and produce very heavy T2-weighted MR images, making it vital for detecting cerebral lesions, such as ischemic stroke, brain tumors, and vascular malformations.[20-22] Moreover, with a fat saturation pulse, fat-saturated FLAIR (fs-FLAIR) can largely reduce the signal of the skull. Although T2 and FLAIR have also been demonstrated to exhibit excellent feasibility in skull-stripping[23,24], few studies have explored the priority of fs-FLAIR in skull-stripping and compared it with that of non-fs FLAIR (nfs-FLAIR).

Based on a deformable model fitting the brain surface via a set of locally adaptive model forces, the brain extraction tool (BET) developed by Smith et al. is a popular and commonly used brain extraction toolkit. Based on intensity estimation of the threshold, BET can essentially separate nonbrain and brain tissues using two adjustable parameters, i.e., fractional threshold intensity and gradient.[25] Moreover, the performance of BET is also quite good when dealing with images of brain tumor.[10] The T1-weighted sequence provides clear gray matter-white matter contrast, and T1-based BET enables effective segmentation of gray matter and white matter. T2-weighted sequences exhibit high contrast between brain tissue and CSF, allowing T2-based BET to offer reliable delineation of the subarachnoid space.[26,27] In this study, we aimed to evaluate a fast and robust method with high accuracy for thick-layer MRI skull stripping of brain tumors based on fs-FLAIR using BET, a method that could be timesaving and easily promoted in clinical practice.

METHODS

This retrospective study was initiated after approval by the institutional review board (IRB). All the activities during the research abided by the basic principles of the Helsinki Declaration, and informed consent was waived.

Patients

Two brain tumor datasets, a glioma group (Group 1) and a meningioma group (Group 2), were retrospectively collected from two different centers. To compare the skull-stripping efficiency of T1, T2 and T1C with that of fs-FLAIR, all patients from the glioma dataset were scanned with fs-FLAIR, T2, T1 and T1C. Moreover, to compare the efficiency of skull stripping based on fs-FLAIR and nfs-FLAIR, the meningioma dataset was scanned with fs-FLAIR (N = 27), nfs-FLAIR (N = 24), T2, T1 and T1C. The detailed MR scanning parameters for the two datasets are provided in Supplement Table 1. Fifty-five patients with gliomas confirmed by pathological examinations were retrospectively enrolled from August 2016 to August 2019. Patients without T1C (N = 5) or fs-FLAIR (N = 4) images were excluded, resulting in the enrollment of 46 glioma patients. Additionally, data from 53 patients with meningioma were retrospectively gathered from June 2017 to May 2020. Patients without T1C (N=1) or with obvious head motion artifacts (N = 1) were excluded, and 51 meningioma patients were ultimately included. The workflow is presented in Figure 1A.

For glioma patients, MR images were acquired using T1 (FLAIR), T2 (FSE), T2 (fs-FLAIR) and T1C (FSE). T1 (FLAIR/FSE), T2 (FSE), T2 (fs-/nfs- FLAIR) and T1C (FLAIR/FSE) sequences were obtained from meningioma patients. Moreover, the scanning parameters of the acquired sequences, including field of view (FOV), repetition time (TR), echo time (TE), slice thickness (ST), slice space (SP), inversion time (IT) and number of excitations (NEX), were recorded. In total, 6 and 5 types of MR scanners were used for the glioma and meningioma datasets. Details of the MR scanners, mp-MRI and scanning parameters are summarized in Supplement Table 1.

Preprocessing

All the obtained DICOM data were first converted to the NIfTI file format[28] using dcm2nii implemented in MRIcron (https://www.mccauslandcenter.sc.edu/crnl/tools). Thereafter, all the images were coregistered to T1C with SPM12 (Wellcome Department of Imaging Neuroscience, London, UK; https://www.fil.ion.ucl.ac.uk/spm/software/spm12/).

Skull stripping

To extract brain tissue, BET was employed to segment nonbrain tissue from an image of the whole head.[25] To test different error tolerance rates of T1, T2, T1C, FLAIR and fs-FLAIR, the fractional intensity threshold ranged from 0.1 to 0.9 with an interval of 0.1. The gold standard

Table 1: Correlation results of Dice's coefficients with scanning parameters at fractional intensity threshold of 0.5

	FOV (mm^2)	TR (ms)	TE (ms)	ST/SP (mm)[c]	IT (ms)	NEX	MR scanner
Glioma Dataset							
T1 (T1-FLAIR)	0.005	-0.05	0.01	0.32*	-0.21	0.16	0.12
T2 (FSE)	-0.07	0.26	-0.50***	-0.18	NA	-0.012	-0.34*
fs-FLAIR	-0.16	0.26	-0.14	0.006	0.15	0.15	-0.20
T1C (T1-FSE)	0.35*	-0.39**	-0.22	-0.08	NA	0.19	0.13
Meningioma Dataset							
T1	-0.14	0.072	-0.034	-0.63***	0.36*	-0.14	-0.21
T2 (FSE)	-0.23	-0.10	-0.39**	-0.24	NA	-0.56***	0.45**
fs-FLAIR[a]	-0.19	0.15	-0.38	NA	-0.26	NA	-0.14
nfs-FLAIR[b]	-0.17	-0.63***	-0.47**	-0.63***	NA	NA	-0.63***
T1C	-0.31*	-0.16	-0.23	0.48***	0.44*	0.28*	0.08

Note: * $0.01 < p \leq 0.05$, ** $0.001 < p \leq 0.01$, and *** $p \leq 0.001$. Abbreviations: FOV – field of view, TR – time of repetition, TE – echo time, ST/SP – slice thickness/slice space, IT – inversion time, NEX – number of excitations, NA – not applicable. Letters a and b indicate that the correlation analysis was implemented using the fs-FLAIR dataset (N=27) and nfs-FLAIR dataset (N=24) of meningiomas. The letter c indicates that the correlation analysis was implemented between Dice coefficients and slice spaces.

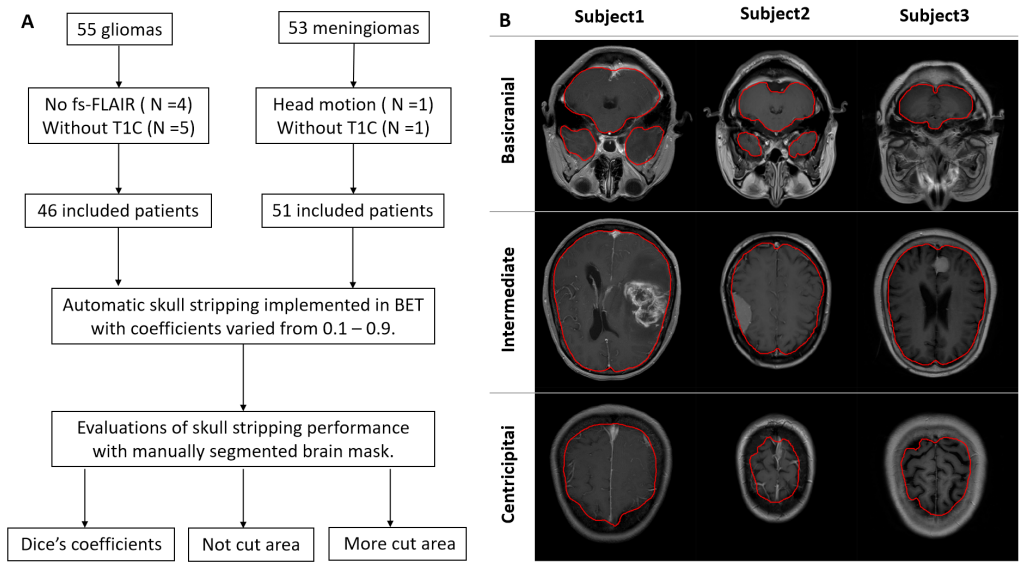

Figure 1. A. Workflow chart of the entire study. B. Representative cases and slices of manually segmented brain areas. Three representative slices of the centricipitai, intermediate and basicranial regions from three subjects are shown. The margin of the segmented brain mask is marked in red and overlaid on T1C images.

of brain extraction, manual segmentation of brain areas by an experienced radiologist, was used to evaluate the skull-stripping efficiency of mp-MRI.

Evaluation metrics

To quantitatively evaluate the brain extraction performance of mp-MRI, a generally used metric, the Dice similarity coefficient, was calculated to assess the segmentation results according to the following equation:

$$\text{Dice} = (\text{TL} \cap \text{GSL})/(\text{TL} \cup \text{GSL}) * 100$$

where TL represents the tested label (TL) and GSL represents the gold standard label (GSL). TL ∩ GSL represents the common portions of two types of labels, and TL ∪ GSL represents the whole areas included in either of the two labels. To obtain a more detailed assessment, the pixel numbers in excessively stripped brain areas and residual nonbrain areas were also counted.

Statistical analysis

All the data are expressed as the mean ± standard deviation. To evaluate the influences of the scanning parameters of mp-MRI with different MR scanners on skull-stripping performance, the correlations between Dice coefficients and MRI scanning parameters were determined using Spearman correlation analysis. To compare the skull-stripping performance of mp-MRI, a paired t test was used to access the differences in the Dice coefficients between fs-FLAIR and other modalities, including T1, T2 and T1C, in both datasets. To determine the differences between fs-FLAIR and nfs-FLAIR in skull stripping, an independent t test was employed. The difference in sex composition between the fs-FLAIR and nfs-FLAIR images within the meningioma dataset was assessed using Fisher's exact test. All the statistical analyses were performed using SPSS version 18.0 (IBM, Armonk, NY, USA), with a two-tailed significance level set at $p \leq 0.05$.

RESULTS

The demographic results of the included datasets

Among the glioma dataset encompassing 46 patients, there were 29 males and 17 females, with a median age of 41 years (from 4 to 67 years). Regarding the meningioma dataset, which included 51 patients, there were 14 males and 37 females, and the median patient age was 53 years (from 5 to 84 years). No significant differences in patients age were detected between the fs-FLAIR and nfs-FLAIR groups (54.07 ± 16.00 vs 52.25 ±12.63, $p = 0.40$). Regarding sex distribution, 17 females and 10 males were included in the fs-FLAIR group, and 20 females and 4 males were included in the nfs-FLAIR group. No significant differences in sex composition were noted between the groups ($p = 0.127$).

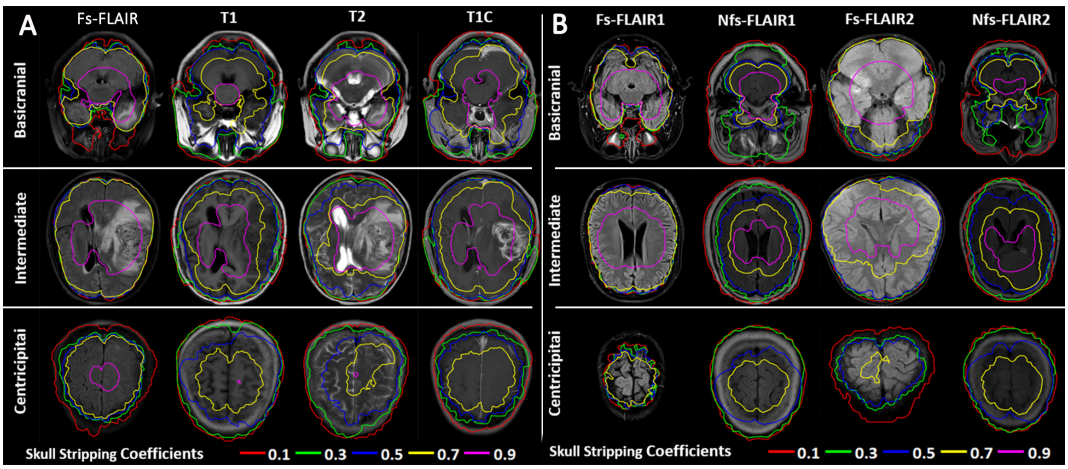

Figure 2A. Representative skull-stripping performance of the mp-MRI of glioma patients. The margins of skull stripped brains (colorful lines listed at the bottom) extracted with different fractional intensity thresholds (from 0.1 to 0.9) were overlapped on different MR modalities. The brain areas extracted with fs-FLAIR at coefficients of 0.3–0.7 exhibited the best match with the brain tissues, and the consistencies were obviously better than those noted for the other modalities. B. Representative slices of the skull-stripping performance of fs-FLAIR and nfs-FLAIR in meningioma patients. The margins of skull-stripped brain areas extracted with different fractional intensity thresholds (from 0.1 to 0.9) were coded with different colored lines and overlapped on the fs-/nfs-FLAIR images. Compared with those extracted with nfs-FLAIR, the brain masks automatically extracted with fs-FLAIR at coefficients of 0.3–0.7 better matched the brain tissues on the centricipitai, intermediate and basicranial slices.

The skull-stripping performance of mp-MRI in brain tumors

The representative skull stripping performances of the two brain tumor datasets are displayed with representative slices in Figure 2. Among all the included mp-MR images, compared with any other modality, fs-FLAIR imaging resulted in better skull-stripping performance. With skull stripping coefficients ranging from 0.1–0.9, skull-stripping with fs-FLAIR obtained the greatest Dice coefficients in both datasets (Figure 3A and 3D), with acceptable levels of areas with no stripping and areas with extra stripping in both the glioma dataset (Figure 3B and 3C) and meningioma dataset (Figure 3E and 3F). Moreover, compared with those obtained with the other modalities, the skull-stripping performance of the fs-FLAIR image manifested smaller variations, with coefficients ranging from 0.3 to 0.7 (Figure 3A and 3D). The skull-stripping performance of the nfs-FLAIR images were comparable to that of the T1, T2 and T1C images. In addition, the differences between the nfs-FLAIR images and the T1, T2 and T1C images were not as obvious as those noted between the fs-FLAIR images (Figure 3D and 3G).

Group-level comparisons of mp-MRI skull stripping

In the glioma dataset, fs-FLAIR demonstrated stable and exact skull-stripping performance. The Dice coefficients for fractional intensity thresholds varied from 0.2 to 0.7 and were greater than 0.80. The maximum was 0.902 at the fractional intensity threshold of 0.6 (Figure 4A–4C), indicating the robustness of fs-FLAIR in skull stripping for brain tumors with thicker-layer images. In contrast, the Dice coefficients of T1, T2 and T1C were mostly less than 0.8, except for a few values of approximately 0.82. All the Dice coefficients of the fs-FLAIR images were significantly greater than those of T1, T2 and T1C, and all the p values were less than 0.0001 (Figure 4A–4C).

With respect to the meningioma dataset, similar skull-stripping performances were found for the fs-FLAIR image (Figure 4D). The maximum Dice coefficient reached 0.87. This value was found in the fs-FLAIR image at a fractional intensity threshold of 0.6. Compared with nfs-FLAIR, fs-FLAIR demonstrated superiority in the skull-stripping performance of brain tumors. In the meningioma dataset, all the Dice coefficients of the fs-FLAIR images were

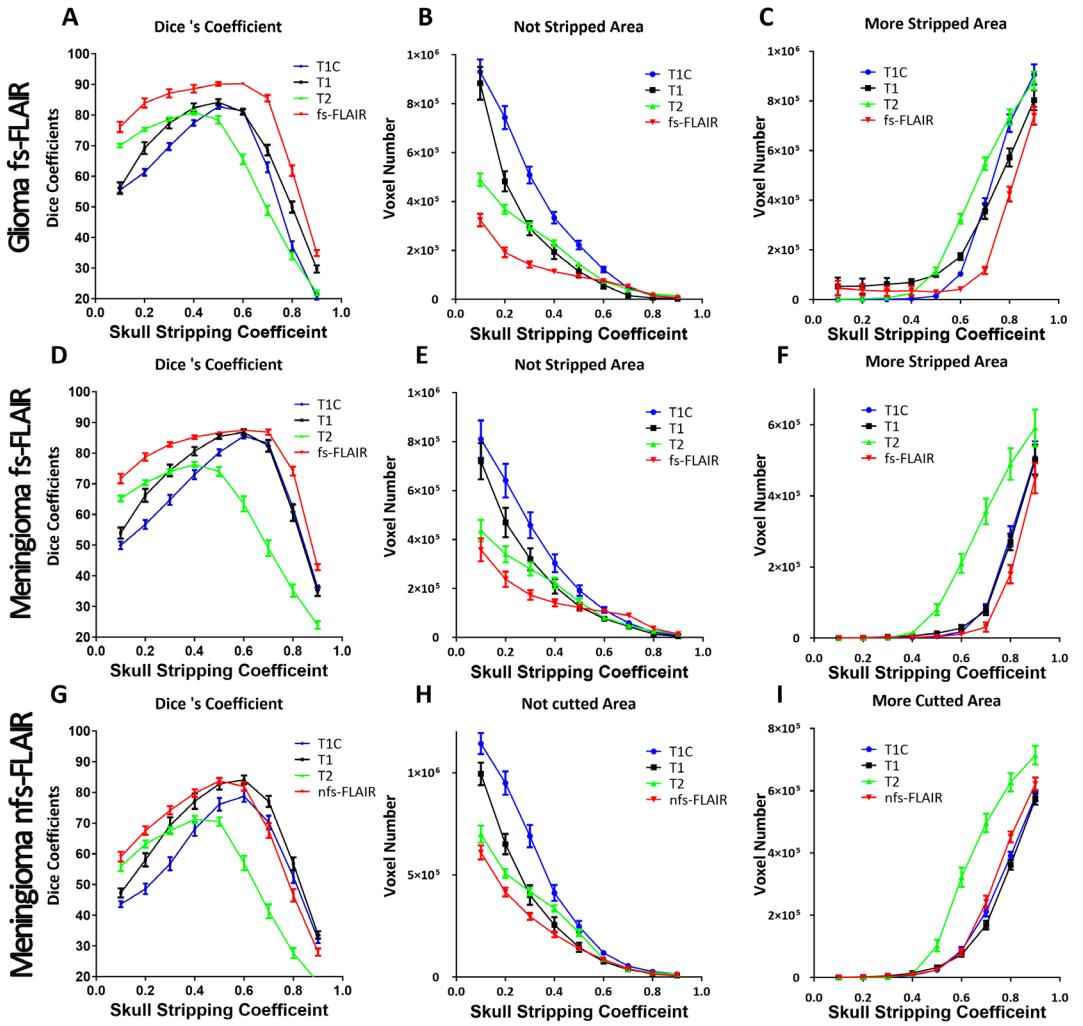

Figure 3. Line graphs of skull-stripping performance in brain tumors. The X axis (**from A to I**) represents the fractional intensity threshold (from 0.1–0.9), and the left Y axis represents the Dice coefficient and/or the number of voxels. Skull-stripping with fs-FLAIR yields the greatest Dice coefficient (**A, D**) and produces both fewer unstripped areas and fewer over stripped areas in the glioma dataset (**B, C**) and meningioma dataset (**E, F**). Skull-stripping with fs-FLAIR manifested less variation (**A, D**); moreover, skull-stripping with nfs-FLAIR was comparable to that obtained with T1, T2 and T1C (**G–I**).

significantly greater than those of the nfs-FLAIR images. Regarding the comparison of fs-FLAIR with other MR modalities, the Dice coefficients of fs-FLAIR were significantly greater than those of T1, T2 and T1C, with the exception of those ofT1 at fractional intensity thresholds of 0.5 and 0.6. Comparisons of Dice coefficients of the meningioma dataset between fs-FLAIR vs. nfs-FLAIR, and fs-FLAIR vs. T1, vs. T2 and vs. T1C were displayed in Figure 4D–4G.

The correlation between Dice coefficient and MR scanning parameters in mp-MRI.

In both the glioma and meningioma datasets, the Dice coefficients of fs-FLAIR showed no significant correlations with all scanning parameters or MR scanners (Table 1). For the other modalities, parameters related voxel numbers and/or image contrast exhibited significant correlations with the performance of skull stripping (Table 1).

In the glioma dataset, slightly significant correlations were observed between the Dice

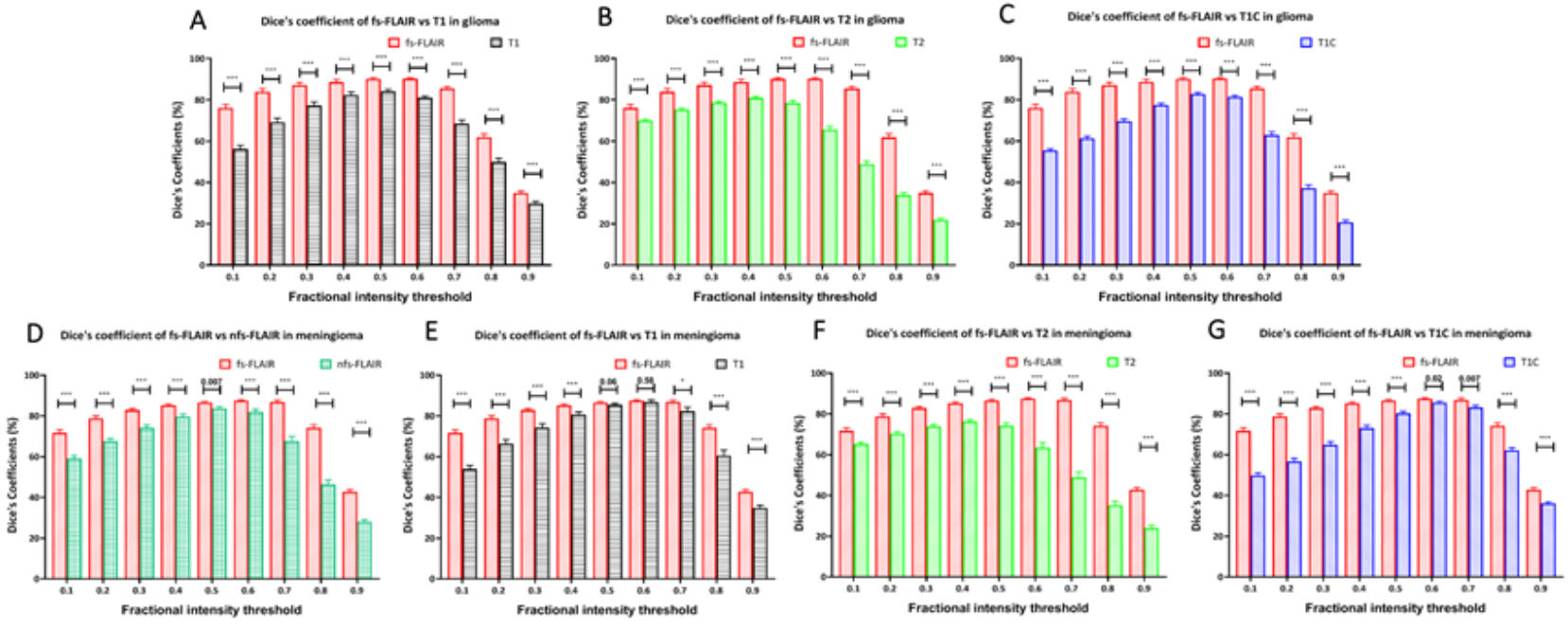

Figure 4. Comparisons of Dice coefficients between fs-FLAIR and T1 (A), between fs-FLAIR and T2 (B) and between fs-FLAIR and T1C (C) in the glioma dataset. Compared with T1, T2 and T1C, Fs-FLAIR has a significantly greater Dice coefficient. Fs-FLAIR achieved high consistency with manually segmented brain areas, demonstrating its priority and stability in skull stripping. Comparisons of the Dice coefficients of fs-FLAIR vs. nfs-FLAIR (D) and fs-FLAIR vs. T1, T2 and T1C (E, F and G) in meningioma dataset. Compared with nfs-FLAIR, T1, T2 and T1C, Fs-FLAIR resulted in significantly greater Dice coefficients, except for a nonsignificant difference in comparison with T1, with coefficients of 0.5 and 0.6, respectively. The extracted brain areas with fs-FLAIR achieved high consistencies with manually segmented brain masks.

coefficients and the ST/SP (r = 0.32, $p < 0.05$) of T1, TE (r = -0.50, $p < 0.0001$) of T2, and TR (r = -0.39, $p < 0.01$) and FOV (r = 0.35, $p < 0.05$) of T1C. For MR scanners, the Dice coefficient exhibited a slightly significant correlation only with T2. In the meningioma dataset, nfs-FLAIR demonstrated much closer and significant correlations with scanning parameters or MR scanner than fs-FLAIR (Max r = -0.63, p < 0.0001, Table 1). Among all parameters, ST/SP manifested the closest correlations with Dice coefficients for T1 and nfs-FLAIR (r = - 0.63, $p <$ 0.0001) as well as a moderate correlation for T1C (Table 1). Moreover, TE of T2 showed significant correlations, whereas NEX of T2 had the highest correlation with Dice coefficients (Table 1). The inversion time of T1 and T1C exhibited slightly significant correlations. Similarly, the Dice coefficient of T2 was slightly significantly correlated with the MR scanner, and this finding is consistent with that noted in the glioma dataset (r = 0.45, $p < 0.01$).

DISCUSSION

In this retrospective study, we demonstrated that fs-FLAIR with BET can serve as a fast and robust approach for skull stripping of brain tumors. Compared with that based on T1, T2, T1C and nfs-FLAIR, automatic brain segmentation based on fs-FLAIR had significantly greater Dice coefficients and was less influenced by MR scanning parameters or MR scanners. Fs-FLAIR displayed more stable and robust skull stripping under a wider fractional intensity threshold range and could serve as a vital tool for skull stripping of brain tumors independent of MR scanners or scanning centers.

Fs-FLAIR enables efficient skull stripping in brain tumor imaging. Brain extractions using fs-FLAIR combined with BET exhibited the greatest consistency with manually segmented brain masks, outperforming those obtained with T1, T2, T1C and nfs-FLAIR sequences. Fs-FLAIR suppresses MR signals from fat and CSF using fat suppression and fluid attenuated inversion recovery techniques. The T2-weighted nature of FLAIR accentuates the cerebral cortex, allowing for more accurate delineation of the boundaries between brain tissue and nonbrain tissue.[20] These characteristics allow BET to distinguish between brain and nonbrain tissues, thereby yielding satisfactory skull-stripping performance. Although gliomas arising from glial cells and meningiomas arising from the meninges differ in histogenesis, comparable skull-stripping performances of fs-FLAIR were observed in both gliomas and meningiomas. Higher Dice coefficients of fs-FLAIR demonstrated less influence of skull stripping with fs-FLAIR based on tumor location or tumor type.

Skull stripping of brain tumors using fs-FLAIR can be performed independently of MR scanners or scanning parameters. Several scanning parameters, including slice thickness, echo time and inversion time, influence skull-stripping performance. Among these, longer inversion times and long-TE readouts could increase the detectability of brain tissue and tissue abnormalities.[19, 29] The increased contrast between nonbrain tissue and brain tissue in fs-FLAIR enables BET to more easily identify the brain margin. BET first calculates the gray histogram of MR images and then estimates the characteristics of the gray histogram to separate brain tissues from nonbrain tissues. Larger differences in signal between brain tissue and nonbrain tissue on fs-FLAIR improve the accuracy of the calculated gray threshold, thus enhancing skull-stripping performance.[30] Considering the excellent performance of MR images with a thinner slice thickness[31], it is reasonable to conclude that skull stripping based on fs-FLAIR with a thinner slice thickness achieves more accurate results than other modalities and is less affected by scanning factors.

T2-weighted MR images with fat saturation for automated brain extraction have also been explored[32, 33], and the excellent agreement between automatically extracted brain volumes partially agreed with our results. However, compared with T2, FLAIR suppresses extracortical or ventricular CSF[34], thus resulting in more accurate skull stripping. Although deep learning-based methods trained on specific sites outperform traditional BET approaches in skull-stripping, they fail to be effectively applied to data from other sites.[35,36] The BET based on fs-FLAIR does not rely on a large data model. In this study, its Dice coefficients showed no significant correlation with any scanning parameters or MR scanners, indicating that it is more widely applicable and practical. Compared with convolutional neural networks, skull stripping with BET has similar accuracies in nonpathological brains.[37] Unlike the relatively low Dice coefficients of BET (0.775) in the tumor dataset in a previous study[37], the accuracy of skull-stripping with fs-FLAIR based on BET was significantly improved in our study. Compared with methods based on atlases[38],

BET is very fast and accurate, and no complex preprocessing, such as registration and/or signal intensity bias correction, needs to be applied.[25] Thus, BET is less influenced by brain templates.[10]

BET has been widely accepted and utilized owing to its high efficacy and user-friendly interface.[25] Given that fs-FLAIR is insensitive to pathological tumor types, MRI scanners and study centers in skull-stripping, it is reasonable to conclude that combining fs-FLAIR with BET could yield a fast, reliable and robust method for the extraction of brain tumors. Previous studies have focused on conventional thick-slice MR images, whereas few studies have focused on fs-FLAIR images.[39] Given that thick-slice MR is widely used in brain tumor imaging, accurate skull stripping based on such images helps integrate large amounts of pre-scanned MR data. These data are valuable for advancing intelligent diagnosis. Fs-FLAIR can contribute to automatic skull stripping, thereby facilitating the translation of artificial intelligence into clinical practice.

Our study has several limitations. First, the scanning parameters were not uniform across our study. However, the accurate and fast automatic skull-stripping performance obtained from fs-FLAIR has demonstrated robustness regardless of the scanning device and sequence parameters, highlighting its broad clinical applicability. Second, the skull striping performance of BET was not compared with that of other methods, such as deep learning. The high consistency obtained in our study encouraged experienced image processing researchers to explore the application value of combining fs-FLAIR with deep learning in the brain extraction. Third, we did not test how BET parameters (beyond the fractional intensity threshold) influence brain extraction outcomes. The optimization of other main BET options, such as bias field correction and neck cleanup, robust brain center estimation, and eye and optic nerve cleanup, could significantly enhance brain extraction performance.

In conclusion, in this study, we investigated the automatic skull-stripping performance of mp-MRI in glioma and meningioma. Compared with T1, T2, T1C and nfs-FLAIR, fs-FLAIR with BET exhibited the optimal skull-stripping performance. Compared with other imaging modalities, fs-FLAIR is less affected scanning factors, such as scanning parameters or MR scanner types. In summary, for conventional thick-layer MRI sequences of brain tumors, automatic skull-stripping based on BET achieves the highest accuracy and fault tolerance in fs-FLAIR. Accordingly, fs-FLAIR can serve as a vital modality in the promotion of the intelligent diagnosis of brain tumors.

DISCLOSURE

Conflict of interest: None

REFERENCES

1. Filho AM, Znaor A, Sunguc C, *et al.* Cancers of the brain and central nervous system: global patterns and trends in incidence. *J Neurooncol* 2025; 172(3):567-78. doi: 10.1007/s11060-025-04944-y.
2. Alsubai S, Khan HU, Alqahtani A, Sha M, Abbas S, Mohammad UG. Ensemble deep learning for brain tumor detection. *Front Comput Neurosci* 2022;16:1005617. doi: 10.3389/fncom.2022.1005617.
3. Huse S, Acharya S, Shukla S, J H, Sachdev A. Computer-aided detection and diagnosis of neurological disorder. *Cureus* 2022;14(8):e28032. doi: 10.7759/cureus.28032.
4. Hoopes A, Mora JS, Dalca AV, Fischl B, Hoffmann M. SynthStrip: skull-stripping for any brain image. *NeuroImage* 2022;260:119474. doi: 10.1016/j.neuroimage.2022.119474.
5. Rempe M, Mentzel F, Pomykala KL, *et al.* k-strip: A novel segmentation algorithm in k-space for the application of skull stripping. *Comput Methods Programs Biomed* 2024;243:107912. doi: 10.1016/j.cmpb.2023.107912.
6. Wang G, Hu Y, Li X, *et al.* Impacts of skull stripping on construction of three-dimensional T1-weighted imaging-based brain structural network in full-term neonates. *Biomed Eng Online* 2020;19(1):41. doi: 10.1186/s12938-020-00785-0.
7. Du W, Yin K, Shi J. Dimensionality reduction hybrid u-net for brain extraction in magnetic resonance imaging. *Brain Sci* 2023;13(11). doi: 10.3390/brainsci13111549.
8. Andrearczyk V, Schiappacasse L, Abler D, *et al.* Automatic detection and multi-component segmentation of brain metastases in longitudinal MRI. *Sci Rep* 2024;14(1):31603. doi: 10.1038/s41598-024-78865-7.
9. Iratni M, Abdullah A, Aldhaheri M, *et al.* Transformers for neuroimage segmentation: Scoping review. *J Med Internet Res* 2025;27:e57723. doi: 10.2196/57723.
10. Fatima A, Shahid AR, Raza B, Madni TM, Janjua UI. State-of-the-art traditional to the machine- and deep-learning-based skull stripping techniques, models, and algorithms. *J Digit Imaging* 2020;33(6):1443-64. doi: 10.1007/s10278-020-00367-5.
11. Iglesias JE, Liu CY, Thompson PM, Tu Z. Robust brain extraction across datasets and comparison with publicly available methods. *IEEE Transactions on Medical Imaging* 2011;30(9):1617-34. doi: 10.1109/tmi.2011.2138152.
12. Ranjbar S, Singleton KW, Curtin L, *et al.* Weakly supervised skull stripping of magnetic

resonance imaging of brain tumor patients. *Front Neuroimaging* 2022;1:832512. doi: 10.3389/fnimg.2022.832512.
13. Sailunaz K, Alhajj S, Özyer T, Rokne J, Alhajj R. A survey on brain tumor image analysis. *Med Biol Eng Comput* 2024;62(1):1-45. doi: 10.1007/s11517-023-02873-4.
14. Pei L, Ak M, Tahon NHM, *et al*. A general skull stripping of multiparametric brain MRIs using 3D convolutional neural network. *Sci Rep* 2022;12(1):10826. doi: 10.1038/s41598-022-14983-4.
15. Bhalodiya JM, Lim CKSN, Arvanitis TN. Magnetic resonance image-based brain tumour segmentation methods: A systematic review. *Digit Health* 2022;8:20552076221074122. doi: 10.1177/20552076221074122.
16. Kim M, Wang JY, Lu W, *et al.* Where does auto-segmentation for brain metastases radiosurgery stand today? *Bioengineering* (Basel) 2024;11(5). doi: 10.3390/bioengineering11050454.
17. Thakur S, Doshi J, Pati S, *et al*. Brain extraction on MRI scans in presence of diffuse glioma: Multi-institutional performance evaluation of deep learning methods and robust modality-agnostic training. *Neuroimage* 2020;220:117081. doi: 10.1016/j.neuroimage.2020.117081.
18. Nishimaki K, Onda K, Ikuta K, *et al*. OpenMAP-T1: A rapid deep-learning approach to parcellate 280 anatomical regions to cover the whole brain. *Hum Brain Mapp* 2024;45(16):e70063. doi: 10.1002/hbm.70063.
19. Hajnal JV, Bryant DJ, Kasuboski L, *et al.* Use of fluid attenuated inversion recovery (FLAIR) pulse sequences in MRI of the brain. *J Comput Assist Tomogr* 1992; 16(6):841-4. doi: 10.1097/00004728-199211000-00001.
20. DiGregorio J, Gibicar A, Khosravani H, *et al*. Cross-sectional and longitudinal Biomarker extraction and analysis for multicentre FLAIR brain MRI. *Neuroimage Rep* 2022;2(2):100091. doi: 10.1016/j.ynirp.2022.100091.
21. Tedyanto EH, Tini K, Pramana NAK. Magnetic resonance imaging in acute ischemic stroke. *Cureus* 2022;14(7):e27224. doi: 10.7759/cureus.27224.
22. Rajinikanth V, Vincent P, Gnanaprakasam CN, Srinivasan K, Chang CY. Brain tumor class detection in Flair/T2 modality MRI slices using elephant-herd algorithm optimized features. *Diagnostics* (Basel) 2023;13(11). doi: 10.3390/diagnostics13111832.
23. Gong T, Han H, Tan Z, *et al.* Segmentation and differentiation of periventricular and deep white matter hyperintensities in 2D T2-FLAIR MRI based on a cascade U-net. *Front Neurol* 2022;13:1021477. doi: 10.3389/fneur.2022.1021477.
24. Buchner JA, Peeken JC, Etzel L, *et al.* Identifying core MRI sequences for reliable automatic brain metastasis segmentation. *Radiother Oncol* 2023; 188:109901. doi: 10.1016/j.radonc.2023.109901.
25. Smith SM. Fast robust automated brain extraction. *Hum Brain Mapp* 2002; 17(3):143-55. doi: 10.1002/hbm.10062.
26. Helms G, Kallenberg K, Dechent P. Contrast-driven approach to intracranial segmentation using a combination of T2- and T1-weighted 3D MRI data sets. *J Magn Reson Imaging* 2006;24(4):790-5. doi: 10.1002/jmri.20692.
27. Chau M, Vu H, Debnath T, Rahman MG. A scoping review of automatic and semi-automatic MRI segmentation in human brain imaging. *Radiography* (Lond) 2025; 31(2):102878. doi: 10.1016/j.radi.2025.01.013.
28. Cox RW, Ashburner J, Breman H, *et al.* A (sort of) new image data format standard: NiFTI-12004.
29. Adams JG, Melhem ER. Clinical usefulness of T2-weighted fluid-attenuated inversion recovery MR imaging of the CNS. *AJR Am J Roentgenol* 1999;172(2):529-36. doi: 10.2214/ajr.172.2.9930818.
30. Raghapriya N, Aswini N, Savitha G. An effective segmentation of MRI images combining threshold and hybrid particle swarm optimization (HPSO-T) for lung, bone and brain (LBB). *SSRG-IJECE* 2024;11(12):92-9. doi: 10.14445/23488549/ijece-v11i12p109.
31. Liu T, Wang Y, Xu Z, *et al*. 3D cube FLAIR plus HyperSense compressed sensing is superior to 2D T2WI FLAIR scanning regarding image quality, spatial resolution, detection rate for cortical microinfarcts. *Medicine* (Baltimore) 2022;101(33):e28659. doi: 10.1097/md.0000000000028659.
32. Haubold J, Pollok OB, Holtkamp M, *et al*. Moving beyond CT body composition analysis: Using style transfer for bringing CT-based fully-automated body composition analysis to T2-weighted MRI sequences. *Invest Radiol* 2025; 60(8):552-9. doi: 10.1097/rli.0000000000001162.
33. Xu P, Lyu J, Lin L, Cheng P, Tang X. LF-SynthSeg: Label-free brain tissue-assisted tumor synthesis and segmentation. *IEEE J Biomed Health Inform* 2025; 29(2):1101-12. doi: 10.1109/jbhi.2024.3489721.
34. Saranathan M, Worters PW, Rettmann DW, Winegar B, Becker J. Physics for clinicians: Fluid-attenuated inversion recovery (FLAIR) and double inversion recovery (DIR) imaging. *J Magn Reson Imaging* 2017; 46(6):1590-600. doi: 10.1002/jmri.25737.
35. Sun Y, Gao K, Wu Z, *et al*. Multi-site infant brain segmentation algorithms: The iSeg-2019 challenge. *IEEE Transactions on Medical Imaging* 2021;40(5):1363-76. doi: 10.1109/tmi.2021.3055428.
36. Azam H, Tariq H, Shehzad D, Akbar S, Shah H, Khan ZA. Fully automated skull stripping from brain magnetic resonance images using mask RCNN-based deep learning neural networks. *Brain Sci* 2023;13(9). doi: 10.3390/brainsci13091255.
37. Kleesiek J, Urban G, Hubert A, *et al*. Deep MRI brain extraction: A 3D convolutional neural network for skull stripping. *Neuroimage* 2016:460-9. doi: 10.1016/j.neuroimage.2016.01.024.
38. Praveenkumar S, Kalaiselvi T, Somasundaram K. Methods of brain extraction from magnetic resonance images of human head: A review. *Crit Rev Biomed Eng* 2023;51(4):1-40. doi: 10.1615/

CritRevBiomedEng.2023047606.
39. DiGregorio J, Arezza G, Gibicar A, Moody AR, Tyrrell PN, Khademi A. Intracranial volume segmentation for neurodegenerative populations using multicentre FLAIR MRI. *Neuroimage Rep* 2021;1(1):100006. doi: 10.1016/j.ynirp.2021.100006.

Supplement Table 1: The detailed parameters of MR scanning protocols in gliomas and meningiomas.

Dataset		FOV (mm^2)	TR (ms)	TE (ms)	ST/SP (mm)	IT (ms)	NEX	MR scanner
Gliomas								
T1 (T1-FLAIR)		180-240	1703-3312	9-25	5/(5-6.5)	689-913	1-2	Achieva, Discovery MR750/750w, Espree, SIGNA Pioneer, TrioTim
T2 (FSE)		180-240	2404-11565	80-134	5/(5-6.5)	NA	1-4	
fs-FLAIR		180-240	8000-10000	86-120	5/(5.5-6)	2400-2567	1-2	
T1C (T1-FSE)		180-240	150-550	2-9	5/(5-6.5)	NA	1-4	
Meningiomas								
T1	T1-FLAIR	230-280	1709-3467	8.5-27	(5,6)/(6.5, 8)	720-1186	1-2	Amira, Discovery MR750, Signa HDxt, SymphonyVision, TrioTim
	T1-FSE	220,230	200-220	2.46, 5	5/6.5	NA	2	
T2 (FSE)		220-250	4000-11004	93-113	(5,6)/(6.5, 8)	NA	1-2	
FLAIR	fs-FLAIR	220-250	6500-9420	84-144	5/6.5	2100-2500	1	
	nfs-FLAIR	240-260	8500-8502	142-162	(5,6)/(6.5-8)	2100	1	
T1C	T1-FLAIR	240-270	1750-3111	20-26	(5,6)/(6.5, 8)	720-1153	1	
	T1-FSE	220, 230	200-663	2-17	5/6.5	NA	1-2	

Abbreviations: FOV – field of view, TR – time of repetition, TE – echo time, ST/SP – slice thickness/slice space, IT – inversion time, NEX – number of excitations, NA–not applicable.